https://doi.org/10.2352/EI.2023.35.6.ISS-347

Implementation of EMVA 1288 Standard Release 4.0 for Characterization of Image Sensors

Meg Borek; Imatest LLC; Boulder, CO

Abstract

The standardization of image sensor characterization allows for a common and comprehensible way to measure, analyze, and present information about various sensors used in the imaging industry. The European Machine Vision Association (EMVA) has developed an industry standard for cameras and sensors applied in the field of machine vision, which is implemented and scrutinized in this paper. The EMVA 1288 Release 4.0 is the most recent version of the standard, going into effect in July 2021 [1], and presents models for the characterization of both linear and non-linear sensors. With the intention of developing standard-compliant analysis software, the fidelity of the newest release—including both linear and general models—is tested by putting standard into practice for a DSLR camera sensor.

Introduction

The EMVA 1288 standard is an initiative to define a unified method for the objective measurement and analysis of specification parameters for image sensors, particularly those used in the computer vision industry. Its goal is to define reliable and reproducible measurement procedures and data presentation guidelines in order to simplify the comparison of cameras and image sensors. Models for both linear and non-linear sensor responses are presented in Version 4.0 of the standard. From image capture to analysis, this paper details the equipment, methodologies, and analyses used in the implementation of the standard, serving as both a proof of concept and an evaluation of the presentation and comprehensibility of the standard guidelines from a user perspective.

Measurements and analyses are made to quantify the linearity, sensitivity, noise, nonuniformity, and dark current of a Canon EOS 40D DSLR sensor (hereafter "Camera 1"), according to the methods described in the EMVA 1288 4.0 standard. This paper details a realistic implementation of these processes and discusses potential flaws and challenges in the standard, as well as complications introduced by non-ideal experimental variables.

Background

The background most relevant to the processes involved is described, including theory and equations applied in the analyses detailed in successive sections. Additional background and derivations can be found in the full EMVA 1288 Release 4.0 standard documentation [1].

Linear and General Models

The linear 4.0 release of the EMVA 1288 standard is only applicable to sensors that adhere to the assumptions of the linear model [1], which assumes that:

1. The sensor has a response that increases linearly with the number of incident photons.
2. The temporal noise is comprised only of dark noise and photon shot noise.
3. Temporal noise between pixels is statistically independent.

In comparison, the general model applies to sensors with non-linear responses or internal reprocessing, and treats the sensor or camera as a black box, assuming that :

1. The characteristic curve (sensor response) is not necessarily linear.
2. The temporal noise includes shot noise plus all unknown noise sources.
3. Temporal noise between pixels is NOT statistically independent.

These and additional assumptions are described in detail in the standard documentation [1]. Data capture processes for both models are identical, such that only the subsequent analyses differ between models.

Sensitivity, Linearity, and Noise

Conversion of Irradiance to Quantum Exposure

The function of an image sensor is to collect photons incident on the pixel array and convert those photons to a digital signal. The average number of photons incident on sensor of area A over exposure time t_{exp} can be calculated when the wavelength-dependent irradiance E at the sensor plane is known as:

$$\mu_p = \frac{A \cdot E \cdot t_{exp}}{h \cdot c/\lambda} \tag{1}$$

where h is Planck's constant and c is the speed of light.

Mean and Variance of Gray Values

Every sensor has several sources of noise which are additive and can often be represented statistically [1]. Shot noise characterizes the fluctuation of electrons in a sensor and is assumed to obey Poisson statistics. Other sources of noise—such as dark noise, quantization noise, and fixed pattern noise—depend on the physical properties of the sensor and its electronics. The average gray value is calculated from two images, $y[0]$ and $y[1]$, captured at the same exposure over $M \times N$ pixels in the active area of the sensor. The average digital count for a single image is given by:

$$\mu_y[k] = \frac{1}{MN} \sum_{M=0}^{M-1} \sum_{N=0}^{N-1} y[k][m][n], (k \in \{0,1\}). \tag{2}$$

The same process is used to find the mean dark values using dark exposure images.

Temporal variance, σ_y^2, is computed from two images:

$$\sigma_y^2 = \frac{1}{2MN}\sum_{M=0}^{M-1}\sum_{N=0}^{N-1}\left(y[0][m][n]-y[1][m][n]\right)^2 - \frac{1}{2}\left(\mu[0]-\mu[1]\right)^2 \tag{3}$$

This method of subtracting the difference of the means eliminates the variance introduced by spatial nonuniformities in the captured images.

Dark Current

Digital sensors introduce some level of the dark signal, μ_d, present even with no light incident on the sensor, typically caused by thermally induced electrons accumulating over time, as described by Eq. 4:

$$\mu_d = \mu_{d.0} + \mu_{therm} = \mu_{d.0} + \mu_{I.y} t_{exp} \tag{4}$$

where $\mu_{d.0}$ is the initial dark signal at exposure time zero, and μ_{therm} is the number of thermally induced electrons per pixel over exposure time t_{exp}. The slope of the linear relationship, $\mu_{I.y}$, is the *dark current* [e^-/pixel/s].

Under the assumption that thermally induced electrons also adhere to a Poisson distribution, the mean μ_{therm} and variance σ^2_{therm} are equal, giving the variance of the dark signal as:

$$\sigma_d^2 = \sigma_{d.0}^2 + \sigma_{therm}^2 = \sigma_{d.0}^2 + \mu_{I.e} t_{exp} \tag{5}$$

which is useful for sensors that include compensation for the dark current [1].

Nonuniformity

Most nonuniformity measurements require averaging over a large number of images, L, in order to reduce the temporal noise below the level of spatial variation [1]. This is done by first averaging together a stack of L images, $\mathbf{y}[l]$,

$$\langle y \rangle = \frac{1}{L}\left(\sum_{L=0}^{L-1} y[l]\right) \tag{6}$$

followed by the averaging over all $M \times N$ pixels in the array.
The spatial variance is then calculated as:

$$s^2_{y.measured} = \frac{1}{MN}\sum_{M=0}^{M-1}\sum_{N=0}^{N-1}\left(\langle y[m][n]\rangle - \mu_y\right)^2 \tag{7}$$

Methods

Three required categories of measurements are defined by the standard, including sensitivity/linearity/noise, dark current, and nonuniformity. A setup in which Camera 1, with no lens, is placed in front of a uniform light source with a circular aperture according to EMVA 1288 standard methodology has been designed and used for data capture at the appropriate distances and light levels, as discussed in successive sections. The settings and capture controls are largely automated using software development kits (SDKs) to ensure the repeatability of crucial variables such as light intensity and exposure time.

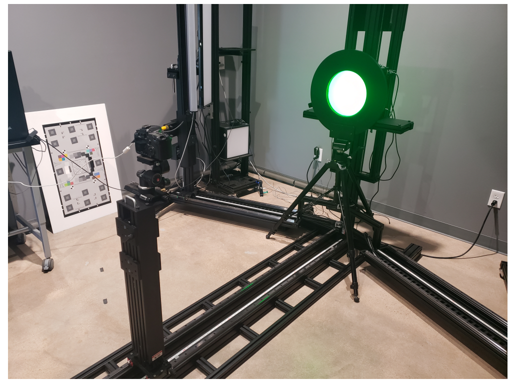

Figure 1: Hardware setup for linearity, sensitivity, and noise measurements. Camera 1 is mounted to a modular test stand at a distance, d, from the light source of adjustable diameter, D, such that the F-number of the system is 8.

Linearity, Sensitivity, and Noise

Light Source Uniformity

Measurements for linearity, sensitivity, and noise require homogeneous illumination of the image sensor. A diffuse, circular light source of diameter, D, illuminates the sensor from a distance, d, where each pixel can receive light from the entire light source using an F-number of 8, such that the active sensor area does not exceed the diameter of the light source. While the use of an integrating sphere is preferred to provide a highly homogeneous light source, it is not required [1]. An available alternative is the Thouslite LED Cube [4]. This tunable light source has 15 individually controllable LED channels covering a spectral range of 350-700 [nm], and the intensity of each channel can be altered via the drive current.

Independently from the standard, a brief uniformity analysis of this source was conducted according to lightbox uniformity procedures outlined by Imatest LLC [2]. For a series of *d/D* combinations, images were captured of the source and analyzed in Imatest software. Distance and size parameters were chosen based on the limitations of the hardware setup. The minimum distance from the source is limited by the 55 [mm] flange distance of the camera body, and the maximum distance is limited by the 2 [m] length of the adjustable slide rail of the Imatest modular test stand [3] on which the camera is mounted. Distances, d, were chosen near the center and the extremes, and corresponding source diameters, D, were calculated to yield an F-number of 8.

Nonuniformity values are averaged across all pixels and channels of the image captures. The best uniformity is achieved at the greatest tested distance, as shown in the summary provided in Table 1.

d [mm]	D [mm]	Avg Nonuniformity (%)
1400	175	4.872
1000	125	6.108
600	75	5.798

Table 1: Calculated nonuniformity values for each set of source diameter and source-sensor distances.

The final hardware setup for linearity, sensitivity, and noise measurements is pictured in Figure 1. A camera or spectrometer can be mounted on the stand and adjusted in the X, Y, and Z directions. The mount is on a slide rail that extends up to 2 meters

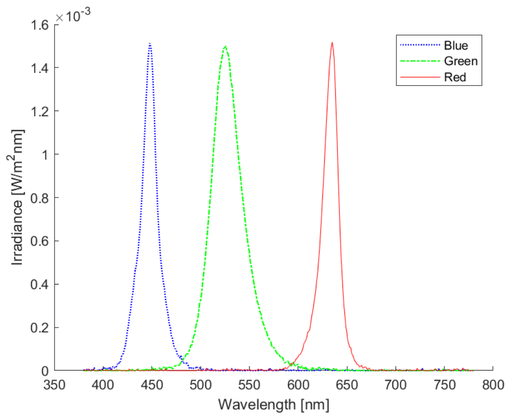

Figure 2: Spectra of the red, green, and blue LED channels used to illuminate the camera sensor

away from the target. The LED light box is mounted to a shelf on the target stand, which has an adjustable height. The camera sensor is placed at a distance of 1400 [mm] away from the light source with a diameter of 175 [mm] to achieve optimal uniformity, and a custom adjustable aperture is mounted in front of the light source to limit the source diameter.

Properties and Calibration of Irradiance

The spectral properties of the irradiation should correspond with the maximum response from the sensor. For multi-channel cameras, multiple forms of irradiation are required for characterizing each channel. The Camera 1 has four channels (RGGB Bayer pattern). A simple experiment was conducted in order to determine which of the available LED channels on the Thouslite source corresponded to the maximum response of each channel. An image was captured at the 1400/175 [mm] distance/diameter configuration determined by the nonuniformity analysis, while the sensor was illuminated by each of the 15 available LED channels on the Thouslite source in succession. For each illumination, the same relative intensity was used. An ISO number of 200, and shutter speed of 1/640 [s] are used for all captures. The red, green (red row), green (blue row), and blue image channels are separated programmatically and analyzed to determine the illumination under which each channel had the greatest response in terms of average digital counts. The greatest responses were achieved by channels with the peak wavelengths included in Table 2.

Channel	Peak λ [nm]
Blue	445
Green (B)	520
Green (R)	520
Red	635

Table 2: Peak wavelengths of each of the Thouslite LED channels that elicited the greatest response from each channel of Camera 1

For data capture, the full-width half-maximum (FWHM) of the illumination should be no more than 50 [nm] [1]. The spectral distribution of each channel is measured using a Jeti Specbos spectrometer positioned on the same plane as the image sensor calibrated in units of irradiance [W/m^2]. Spectra are shown in Figure 2. Irradiance is converted to mean photons reaching the sensor at each exposure time, for each channel, using Eq. 1.

Dark Current

EMVA 1288 only requires that dark current be evaluated at a single temperature, although optional measurements can be performed at varying temperatures to determine the temperature dependency. This process requires the use of a climate exposure chamber or similar hardware, which was not available for these experiments, and therefore was not tested in this study.

Single Temperature Dark Current Evaluation

Measurements for dark current at a single temperature were conducted in a lab setting at room temperature of 22 degrees Celsius. The dark current can be measured using both the mean and the variance of the dark gray value, according to Eqs. 4 and 5, respectively. Using Camera 1, dark images were captured for all available shutter speeds, from 1/8000 up to 30 [s]. Similarly to the linearity and sensitivity measurements, an ISO of 200 was used, and two images are captured for each exposure time.

Nonuniformity

Data capture for spatial nonuniformity is conducted under the same conditions as the linearity, sensitivity, and noise measurements. Quantities related to most nonuniformities are evaluated using the mean gray values averaged over a large number of images in order to suppress temporal noise [1]. The analysis is completed using an averaged set of dark images and an averaged set of images that are 50% saturated. These averages yield $\langle y_{dark} \rangle$ and $\langle y_{50} \rangle$, which are computed using Eq. 6.

A constant shutter speed of 1/60 [s] is used to capture both dark and half-saturation images for the blue, green, and red channels. To achieve 50% saturation under the various illuminations, intensity values were adjusted for each illumination to achieve a mean digital number that was 50% of the maximum saturation. For a 14-bit sensor, saturation occurs at 16225 [DN], so half-saturation images with a mean of 8112 [DN] were captured. One hundred dark images were captured in addition to one hundred half-saturation images under each illumination.

Data Analysis and Results

Linearity, Sensitivity, and Noise

Photon Transfer Curve

The photon transfer curve, shown for each channel in Figure 3, represents the relationship between mean photon-induced gray values and the corresponding variance. The slope of this curve is the gain, K, or amplification of the system, described by

$$\sigma_y^2 = \sigma_{y.dark}^2 + K\left(\mu_y - \mu_{y.dark}\right) \quad \text{Photon Transfer Curve} \quad (8)$$

where μ_y is the average gray value over all pixels in an image captured at a particular time. The mean is computed from the two images captured at the same exposure time according to Eq. 2. This process is also applied to the dark images, yielding $\mu_{y.dark}$. From these same images, the temporal variance σ_y^2 is calculated via Eq. 3 and similarly for the darks to determine $\sigma_{y.dark}^2$.

Gain is a quantity used to describe camera electronics related to the conversion of photons to a voltage, which is amplified and converted into a digital signal. For a linear process as shown, there is a single gain value, or slope, that describes the system. Each channel is analyzed separately due to wavelength dependencies, including each of the two green channels to identify discrepancies. It is not expected for any digital imaging sensor to

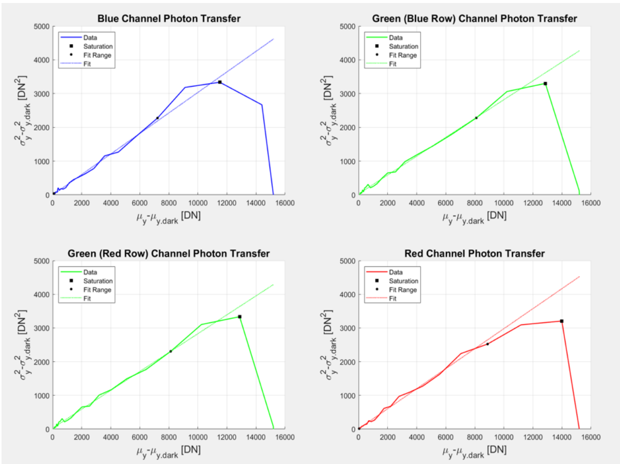

Figure 3: Photon transfer curves for each of of the four channels of Camera 1

be perfectly linear due to inevitable sources of error and noise. The linear trend deviates upon nearing, and eventually fails at, the point of saturation, as shown in Figure 3. To obtain a single slope value for the gain, a linear regression is fitted to the data ranging from the minimum value up to 70% of the value of saturation. For nonlinear systems, due to the black box nature of the system, the photon transfer curve—and therefore the gain—can not be calculated.

Characteristic Curve

The sensitivity, or characteristic curve, shown for each channel in Figure 4, is the relationship between the mean gray value and mean number of photons per pixel. The slope of this curve yields the responsivity, R.

Linear Model

In the linear model, this relation is described as

$$\mu_y - \mu_{y.dark} = R\mu_p \quad \text{Characteristic Curve} \tag{9}$$

where μ_y and $\mu_{y.dark}$ are the average gray values calculated using Eq. 2. μ_p is the quantum exposure, in photons, which is calculated from the radiance at the sensor plane according to Eq. 1. This curve, shown in Figure 4, is fitted using a linear least square regression.

The ratio of these two resultant quantities—responsivity, R, over gain, K—yields the quantum efficiency, η:

$$\eta = \frac{R}{K} \tag{10}$$

which is the percentage of photons incident on a photodiode that generates an electric charge. QE and gain are also used in the final calculation of SNR in Eq. 12.

General Model

Because the general model can be used for non-linear response sensors, the characteristic curve is fitted using a cubic B-spline regression in the form:

$$\mu_y - \mu_{y.dark} = \sum_{p=0}^{P+2} \alpha_p \beta_3 \left(\frac{\mu_p}{\Delta\mu_p} - (p-1) \right) \tag{11}$$

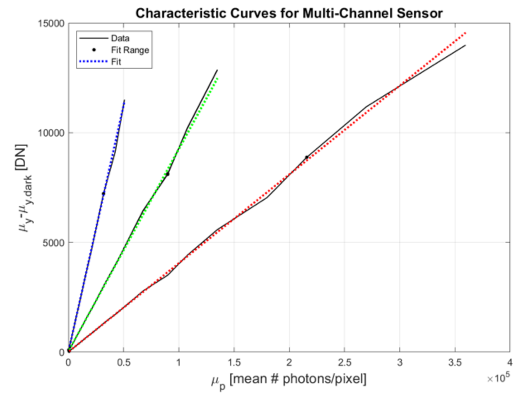

Figure 4: Photon transfer curves, also called sensitivity curves, for each of the four channels of Camera 1

where α_p are the regression parameters for the cubic B-splines, β_3, fit to the curve over P intervals of width $\Delta\mu_p = \mu_{p.sat}/P$. The photon-dependent responsivity is the instantaneous slope, or derivative, of the curve.

Dark Current

Dark current can be computed from either the mean or the variance, using Eqs. 2 and 3, respectively. The mean is preferred because it can be more accurately estimated, but the variance calculation is useful for systems that feature dark current compensation, which is not dealt with in these experiments. The resulting mean dark signal [DN] and the variance in dark signal [DN^2] are plotted against exposure time in Figure 5. The slope of the mean dark signal relation is the dark current, which is determined by performing a linear least squares regression on the data points.

Nonuniformity

The last set of required measured measurements for the standard involves the characterization of sensor nonuniformities. Figure 6 shows a scaled image captured by Camera 1 at 50% saturation. The dark circular spots show the dust on the sensor, and there is obvious vignetting around the edges and corners. Of particular interest are the vertical lines visible in the image. This is common in most digital sensors. In charge-coupled device (CCD) sensors, it is due to charge transfer during readout. In complementary metal–oxide–semiconductor (CMOS) sensors, such as the one in the camera used to capture this image, these lines are usually the result of fixed pattern noise. Many CMOS sensors exhibit this noise because the sensor has individual amplifiers on each column. Slight differences in amplification across columns of pixels result in these variations in the output signal. The objective

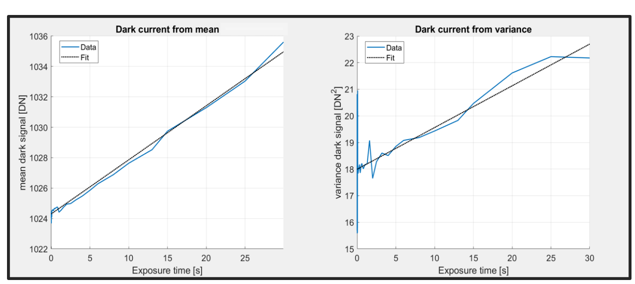

Figure 5: Dark current calculated from mean and variance.

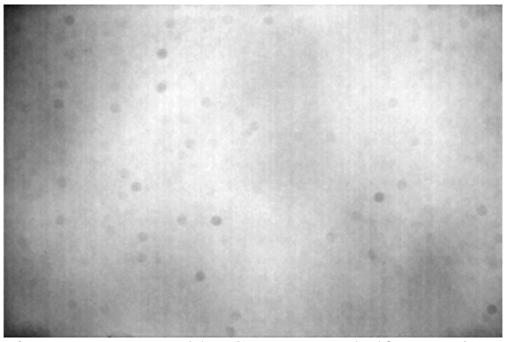

Figure 6: Image captured by Camera 1 at half-saturation, scaled to reveal the extent of nonuniformities of the sensor including vignetting, dust specks, and fixed pattern noise.

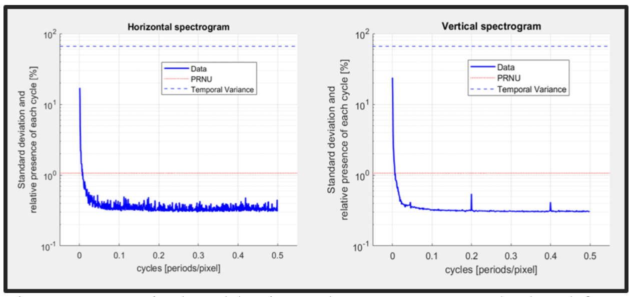

Figure 7: Vertical and horizontal spectrograms calculated from the 50% saturation images for the blue channel

characterization of the nonuniformity utilizes a descriptor called photo-response nonuniformity (PRNU), which describes the variation in gain across a sensor by analyzing the frequency information of the captured images. Spectrograms, such as those shown in Figure 7, are calculated by taking the one-dimensional Fourier transform of an image in either the horizontal or vertical direction, and then computing the mean power spectrum (in the corresponding direction) of that result. As before, all of these calculations are done for each channel. In Figure 7, short peaks that are visible in the vertical spectrogram correspond with the frequencies of the column noise.

A similar computational process is applied to the series of dark captures to yield dark-signal nonuniformity (DSNU). Figure 8 shows a dark image captured with Camera 1, scaled to make the noise more apparent. Close examination reveals hot pixels, which appear fully saturated, and a horizontal banding pattern. Corresponding spectrograms are shown in Figure 9.

SNR Analysis

All of these measurements and quantities come together in the calculation of the total SNR. Eq. 12 for the linear model incorporates quantum efficiency, η, the incident number of photons, μ_p, temporal dark noise, σ_d^2, the DSNU and PRNU, gain, K, and readout noise, σ_q^2.

$$SNR_{tot}(\mu_p) = \frac{\eta \mu_p}{\sqrt{\sigma_d^2 + DSNU^2 + \frac{\sigma_q^2}{K^2} + \eta \mu_p + PRNU^2 (\eta \mu_p)^2}} \tag{12}$$

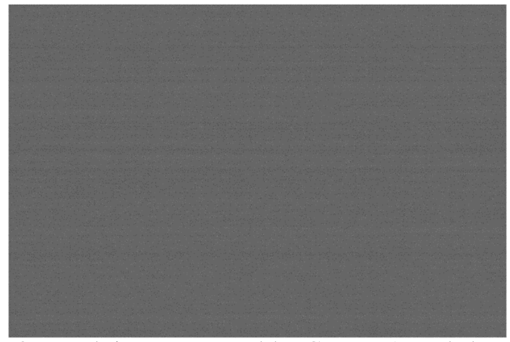

Figure 8: Dark image captured by Camera 1, scaled to reveal the extent of nonuniformities of the sensor. Close examination reveals hot pixels and a vertical banding pattern.

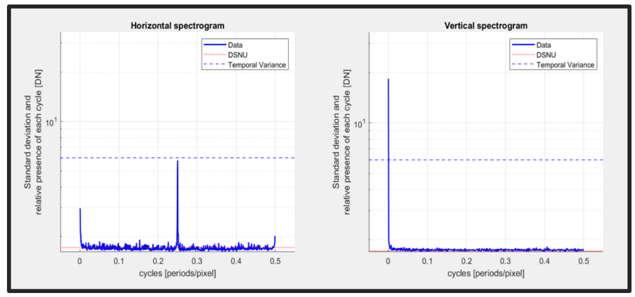

Figure 9: Vertical and horizontal spectrograms calculated from dark images for each channel

Without known efficiency or gain values, the total SNR for the general model is calculated as:

$$SNR_{p.tot}(\mu_p) = \frac{\mu_p}{\sqrt{\sigma_p^2(\mu_p) + s_p^2(\mu_p)}} \tag{13}$$

Linear SNR curves for the blue channel of the Camera 1 are plotted in Figure 10. Notice that when taking into account the DSNU and PRNU in the total SNR, there is a falloff in SNR as the irradiation increases and approaches saturation, as opposed to the theoretical SNR. Equations for the various forms of SNR are defined in the standard documentation [1].

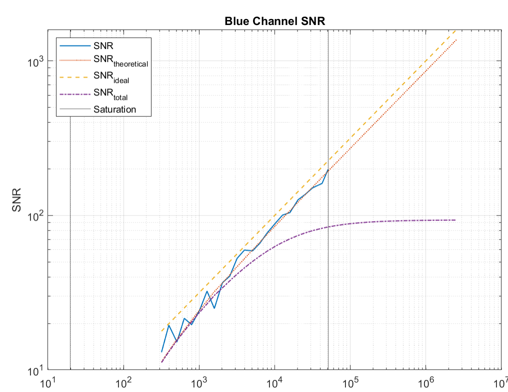

Figure 10: Signal-to-Noise Ratio (SNR) analysis for blue channel based on combination of calculated parameters. Increased variation in the SNR at lower irradiation is due to the larger number of data points taken at shorter exposure times.

Additional Experimentation and Discussion
Challenges
Interpretation of standard instructions

The implementation of any standard can raise challenges due to interpretation of instructions. Certain portions of the standard in particular, such as the nonuniformity analyses, have missing or vague instructions that required a significant amount of trial and error in order to achieve the expected results. A notable example of this occurred during the computation of the spectrograms in the nonuniformity analysis. The standard states that an uneven illumination correction should be applied to the captured images via filtering, however, after doing so, the resulting spectrograms were not consistent with the examples included in the data. Upon referencing back to version 3.1 of the standard, it was evident that the filtering step should not be applied for the computation of the spectrograms, but this is not mentioned in version 4.0. The standard also does not specify how to handle edges during filtering, and some published plots have incorrect labels that affect the expected results.

Hardware limitations

Realistic implementation of the standard requires creative solutions to challenges presented by the limitations of the sensor and measurement hardware. Using a DSLR camera presented the issue of fixed exposure times that were not equally spaced as specified by the standard. As a result, although the initial dataset—which captures linearity and sensitivity measurements under constant illumination at only the available exposure times using the camera—yields good and expected results, it is still not the most accurate implementation of the standard.

This led to the collection of an additional dataset in which a constant exposure time of 1/60 [s] was used in conjunction of variable intensity of the illumination. This in itself presented unique challenges due to the necessity of acquiring spectral measurements of the light source at each of the intensity values used. The same linearity and sensitivity analyses were conducted for an additional set of images captured at equally spaced radiant exposure values, again for each of the color channels in the sensor. The same parameters and setup were used to capture the data including sensor-source distance, source aperture, and ISO number, with the exception of the method of exposure variation.

The resulting photon transfer curve for the blue channel is compared with that of the initial data set in Figure 11. Comparison of the results from both data sets reveals slight differences in the output gain and responsivity values, summarized in Table 3, despite these methods of variation being theoretically equivalent. These discrepancies may be indicative of error introduced by the illumination variation process via the adjustable drive current, differences in the spacing of measured radiant exposures between data sets, or potential reciprocity law failure.

Conclusion

As with many standards, EMVA 1288 has nuances and real-world limitations that inevitably lead to the introduction of error, affecting the accuracy of results. Users of the standard who do not have access to the EMVA characterization setup are limited by their available hardware and software implementations—challenges that this work intends to highlight and begin to find solutions for. By implementing the standard from image capture to analysis, we have a better understanding of problems that may arise during the process and effects that various interpretations and implementations of the standard have on the results.

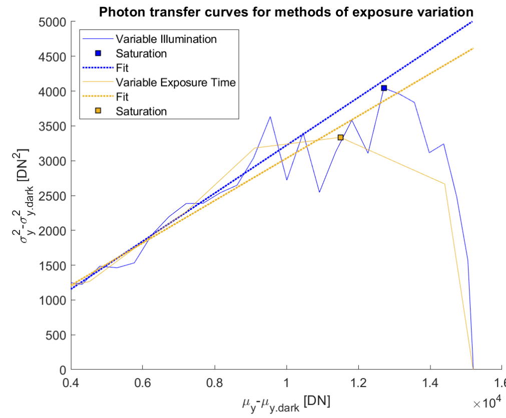

Figure 11: Comparison of photon transfer curves for the same sensor, but different methods of radiant exposure variation.

	Constant Illumination w/ Variable Exposure Time		Constant Exposure Time w/ Variable Illumination	
Channel	Gain [DN/e-]	Responsivity [DN/photon]	Gain [DN/e-]	Responsivity [DN/photon]
B	0.344	0.211	0.304	0.225
G(B)	0.322	0.171	0.279	0.092
G(R)	0.325	0.171	0.280	0.092
R	0.313	0.063	0.297	0.064

Table 3: Comparison of calculated gain and responsivity values for different methods of radiant exposure variation.

References

[1] "EMVA 1288 standard for characterization of image sensors and cameras." [Online]. Available: https://www.emva.org/standards-technology/emva-1288/

[2] "Lightbox uniformity comparison," Jan 2018. [Online]. Available: https://www.imatest.com/2018/01/lightbox-uniformity-comparison/how

[3] "Imatest modular test stand," Jun 2019. [Online]. Available: https://www.imatest.com/product/imatest-modular-test-stand/

[4] "Thouslite ledcube lamp; fixture," Aug 2021. [Online]. Available: https://www.imatest.com/product/thouslite-ledcube-fixture-package/

[5] B. Jahne, "Simulated camera data for EMVA 1288 verification," 2021. [Online]. Available: https://hci.iwr.uni-heidelberg.de/Simulated Camera Data for EMVA 1288 Verification

Author Biography

Meg Borek received her BS in Imaging Science from the Rochester Institute of Technology (2022), where her studies focused on remote sensing, image processing and computer vision, and image sensor analysis. She currently works as an Imaging Scientist at Imatest LLC in Boulder, CO, where her work is focused on imaging standards, software development, and test lab services.